Event-Based Communication Strategy for Collaborative Navigation with Signals of Opportunity

Joshua Morales and Zaher M. Kassas
Department of Electrical and Computer Engineering
University of California, Riverside
{jmora047@ucr.edu, zkassas@ieee.org}

***Abstract*—An event-based communication strategy for collaborative navigation with signals of opportunity (SOPs) is developed. The following problem is considered. Multiple vehicles draw pseudorange measurements from ambient terrestrial SOPs. The vehicles transmit to each other a packet containing pseudoranges to SOPs, in order to collaboratively estimate the vehicles' and SOPs' states. Instead of transmitting this at a fixed communication rate, an event-based strategy is developed to communicate this packet, where the communication event is triggered whenever the maximum position error could violate a desired threshold by a user-specified probability. Simulation results are presented for an environment with four unmanned aerial vehicles (UAVs) and six SOPs, demonstrating an 86.2% reduction in the cumulative communicated data over a fixed-rate strategy. Experimental results with 2 UAVs and 3 SOPs are shown to reduce the cumulative communicated data by 10.3%.**

I. Introduction

Today's navigation systems mainly rely on a global navigation satellite system (GNSS) receiver for positioning. However, GNSS signals often become unusable (e.g., in deep urban canyons or in the presence of interference or jamming). Recently, the exploitation of signals of opportunity (SOPs) have been shown to be an attractive alternative for navigation when GNSS signals become unusable [1], [2]. SOPs (e.g., AM/FM radio [3], cellular [4], digital television [5], and low Earth orbit (LEO) satellites [6]) are attractive for navigation because their signals are: received at a high power, transmitted at high bandwidths, and are geographically abundant and geometrically diverse.

Collaboration is known to improve the navigation performance [7], [8]. Collaborating vehicles can improve estimates of their individual states (position, velocity, clock bias, and clock drift) by sharing and fusing mutual measurements made on SOPs [9], [10]. However, transmitting data between other collaborating vehicles requires a large communication bandwidth and compromises privacy. To address these concerns, this paper develops an event-based communication strategy that aims to reduce the amount of data that vehicles communicate while maintaining a specified estimation uncertainty. Event-based communication strategies have been studied in other contexts and have lead to different event-triggering tests, such as: level-triggering, which compares the amplitude of a signal versus a pre-defined threshold [11]; average estimation error covariance minimization, which checks the average of the time-history of the trace of the estimation error covariance [12]; residual-based, which checks the difference between the measurement and predicted measurement [13]; and innovation error variance-based tests [14]. In this paper, the vehicles will only exchange information if the predicted position estimation uncertainty would violate a specified threshold if information exchange does not take place. This strategy is compared with a fixed-rate communication strategy in which the vehicles communicate at each measurement epoch. The proposed event-based strategy is demonstrated to significantly reduce the transmitted data bits, while maintaining a specified estimation uncertainty.

The remainder of this paper is organized as follows. Section II describes the dynamics model of the SOPs and navigating vehicles as well as the pseudorange measurement model. Section III describes and demonstrates the event-based communication strategy. Section IV presents simulation results with four unmanned aerial vehicles (UAVs) and six SOPs, showing the developed event-based strategy reducing the cumulative communicated data by 86.2% from a fixed-rate strategy. Section V presents experimental results with two UAVs and three cellular SOPs. Concluding remarks are given in Section VI.

This work was supported in part by the Office of Naval Research (ONR) under Grant N00014-16-1-2305 and in part by the National Science Foundation (NSF) under Grant 1566240 and Grant 1751205.

II. Model Description

A. SOP Dynamics Model

Each of the M SOPs will be assumed to emanate from a spatially-stationary terrestrial transmitter, and its state vector $\boldsymbol{x}_{s_m}$ will consist of its planar position states $\boldsymbol{r}_{s_m} \triangleq [x_{s_m}, y_{s_m}]^\mathsf{T}$ and clock error states $\boldsymbol{x}_{\text{clk},s_m} \triangleq c\left[\delta t_{s_m}, \dot{\delta t}_{s_m}\right]^\mathsf{T}$, where c is the speed of light, δt_{s_m} and $\dot{\delta t}_{s_m}$ are the clock bias and drift of the m^{th} SOP transmitter, respectively.

The discretized SOP transmitters' dynamics are given by

$$\boldsymbol{x}_{s_m}(k+1) = \mathbf{F}_s\, \boldsymbol{x}_{s_m}(k) + \boldsymbol{w}_{s_m}(k), \quad k = 1, 2, \ldots,$$

$$\boldsymbol{x}_{s_m} = \left[\boldsymbol{r}_{s_m}^\mathsf{T}, \boldsymbol{x}_{\text{clk},s_m}^\mathsf{T}\right]^\mathsf{T},$$

$$\mathbf{F}_s = \mathrm{diag}\left[\mathbf{I}_{2\times 2},\, \mathbf{F}_{\mathrm{clk}}\right], \quad \mathbf{F}_{\mathrm{clk}} = \begin{bmatrix} 1 & T \\ 0 & 1 \end{bmatrix},$$

where T is the constant sampling interval and $\boldsymbol{w}_{s_m}$ is the process noise, which is modeled as a discrete-time white noise sequence with covariance $\mathbf{Q}_{s_m} = \mathrm{diag}\left[\mathbf{0}_{2\times 2},\, c^2\mathbf{Q}_{\mathrm{clk},s_m}\right]$, where

$$\mathbf{Q}_{\mathrm{clk},s_m} = \begin{bmatrix} S_{\tilde{w}_{\delta t_{s,m}}} T + S_{w_{\dot{\delta} t_{s,m}}} \frac{T^3}{3} & S_{\tilde{w}_{\dot{\delta} t_{s,m}}} \frac{T^2}{2} \\ S_{\tilde{w}_{\dot{\delta} t_{s,m}}} \frac{T^2}{2} & S_{\tilde{w}_{\dot{\delta} t_{s,m}}} T \end{bmatrix}.$$

The terms $S_{\tilde{w}_{\delta t_{s,m}}}$ and $S_{\tilde{w}_{\dot{\delta} t_{s,m}}}$ are the clock bias and drift process noise power spectra, respectively, which can be related to the power-law coefficients, $\{h_{\alpha,s_m}\}_{\alpha=-2}^{2}$, which have been shown through laboratory experiments to characterize the power spectral density of the fractional frequency deviation of an oscillator from nominal frequency according to $S_{\tilde{w}_{\delta t_{s,m}}} \approx \frac{h_{0,s_m}}{2}$ and $S_{\tilde{w}_{\dot{\delta} t_{s,m}}} \approx 2\pi^2 h_{-2,s_m}$ [15].

B. Vehicle Dynamics Model

The n^{th} vehicle's planar position $\boldsymbol{r}_{r_n} \triangleq [x_{r_n},\, y_{r_n}]^{\mathsf{T}}$ and velocity $\dot{\boldsymbol{r}}_{r_n}$ will be assumed to evolve according to an arbitrary, but known, linear dynamics model (e.g., velocity random walk or constant turn rate [16]). The vehicle's state vector $\boldsymbol{x}_{r_n}$ is defined by augmenting the vehicle's position and velocity states $\boldsymbol{x}_{\mathrm{pv}_n} \triangleq \left[\boldsymbol{r}_{r_n}^{\mathsf{T}},\, \dot{\boldsymbol{r}}_{r_n}^{\mathsf{T}}\right]^{\mathsf{T}}$ with the vehicle-mounted receiver's clock error states, $\boldsymbol{x}_{\mathrm{clk},r_n} \triangleq c\left[\delta t_{r_n},\, \dot{\delta t}_{r_n}\right]^{\mathsf{T}}$, i.e., $\boldsymbol{x}_{r_n} \triangleq \left[\boldsymbol{x}_{\mathrm{pv}_n}^{\mathsf{T}},\, \boldsymbol{x}_{\mathrm{clk},r_n}^{\mathsf{T}}\right]^{\mathsf{T}}$. Discretizing the vehicle's dynamics at a constant sampling period T yields

$$\boldsymbol{x}_{r_n}(k+1) = \mathbf{F}_{r_n}\boldsymbol{x}_{r_n}(k) + \boldsymbol{w}_{r_n}(k),$$

$$\mathbf{F}_{r_n} \triangleq \mathrm{diag}\left[\mathbf{F}_{\mathrm{pv}_n},\, \mathbf{F}_{\mathrm{clk}}\right],$$

where $\mathbf{F}_{\mathrm{pv}_n}$ is the position and velocity state-transition matrix, and $\boldsymbol{w}_{r_n}$ is the process noise vector, which is modeled as a discrete-time zero-mean white noise sequence with covariance $\mathbf{Q}_{r_n} = \mathrm{diag}\left[\mathbf{Q}_{\mathrm{pv}_n},\, c^2\mathbf{Q}_{\mathrm{clk},r_n}\right]$, where $\mathbf{Q}_{\mathrm{pv}_n}$ is the position and velocity process noise covariance and $\mathbf{Q}_{\mathrm{clk},r_n}$ is identical to $\mathbf{Q}_{\mathrm{clk},s_m}$, except that $S_{\tilde{w}_{\delta t_{s,m}}}$ and $S_{\tilde{w}_{\dot{\delta} t_{s,m}}}$ are now replaced with receiver-specific spectra, $S_{\tilde{w}_{\delta t_{r,n}}}$ and $S_{\tilde{w}_{\dot{\delta} t_{r,n}}}$, respectively.

C. Pseudorange Measurement Model

The pseudorange measurements made by the n^{th} receiver on the m^{th} SOP, after discretization and mild approximations discussed in [17], are modeled as

$$\begin{aligned} {}^{n}z_{s_m}(k) &= \|\boldsymbol{r}_{r_n}(k) - \boldsymbol{r}_{s_m}\|_2 \\ &\quad + c\cdot[\delta t_{r_n}(k) - \delta t_{s_m}(k)] + {}^{n}v_{s_m}(k), \end{aligned} \tag{1}$$

where ${}^{n}v_{s_m}$ is the measurement noise, which is modeled as a discrete-time zero-mean white Gaussian sequence with variance ${}^{n}\sigma_{s_m}^2$.

III. Event-based Collaborative Opportunistic Navigation Framework

This section develops an extended Kalman filter (EKF)-based collaborative navigation framework that uses an event-based communication strategy to transmit data between vehicles.

A. Framework Overview

In this framework, the positions of all SOPs $\{\boldsymbol{r}_{s_m}\}_{m=1}^{M}$ are assumed to be known *a priori* (e.g., via radio mapping [18]), while the clock states of the SOPs are continuously estimated along with the states of the navigating vehicles. This can be achieved through an EKF with state vector

$$\boldsymbol{x} \triangleq \left[\boldsymbol{x}_{r_1}^{\mathsf{T}}, \ldots, \boldsymbol{x}_{r_N}^{\mathsf{T}},\, \boldsymbol{x}_{\mathrm{clk},s_1}^{\mathsf{T}}, \ldots, \boldsymbol{x}_{\mathrm{clk},s_M}^{\mathsf{T}}\right]^{\mathsf{T}}.$$

At each measurement epoch, each vehicle transmits a packet $\boldsymbol{\Lambda}_n$ of SOP pseudoranges, namely

$$\boldsymbol{\Lambda}_n(k+1) \triangleq \{{}^{n}\boldsymbol{z}_s(k+1)\}, \tag{2}$$

where

$${}^{n}\boldsymbol{z}_s = [{}^{n}z_{s_1}, \ldots, {}^{n}z_{s_M}]^{\mathsf{T}}.$$

Then, each vehicle fuses all received packets with its own measurements to estimate $\boldsymbol{x}$. Fig. 1 illustrates a high-level diagram of the collaborative navigation framework, where τ is always closed in a traditional fixed-rate communication strategy. Note that in such case, this framework is identical to a centralized EKF architecture, since each vehicle is estimating $\boldsymbol{x}$ and all vehicles communicate their data in a fully-connected graph. Previous work focused on minimizing the data in the communicated packets $\{\Lambda_n\}_{n=1}^{N}$ [19] and studying the robustness due to packet drops in lossy communication channels [10]. This paper will devise an event-based communication strategy to transmit $\{\Lambda_n\}_{n=1}^{N}$ (i.e., τ closes only when needed).

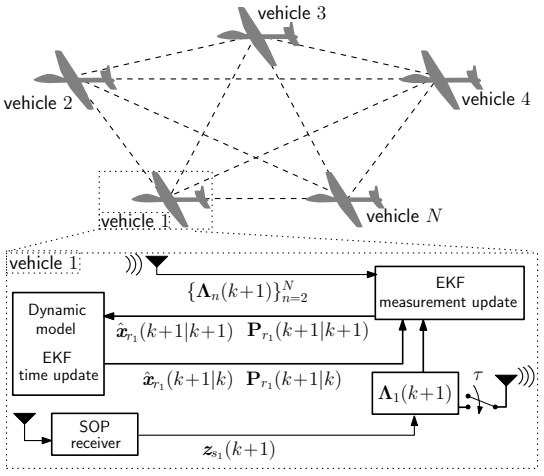

Fig. 1. Collaborative navigation with SOPs. If τ is always closed, the packets $\{\boldsymbol{\Lambda}_n\}_{n=1}^{N}$ are transmitted at every measurement epoch (i.e., at a fixed rate). The event-based strategy will devise a mechanism to close τ only when needed.

The EKF time update step, the event-based communication strategy, and the EKF measurement update are discussed next.

B. EKF Time Update

The EKF time update produces $\hat{\boldsymbol{x}}(k{+}1|k) \triangleq \mathbb{E}[\boldsymbol{x}(k{+}1)|\boldsymbol{Z}^k]$, where $\mathbb{E}[\,\cdot\,|\,\cdot\,]$ is the conditional expectation operator, $\boldsymbol{Z}^k \triangleq \{\boldsymbol{z}(i)\}_{i=1}^k$, and

$$\boldsymbol{z} \triangleq \left[{}^1\boldsymbol{z}_s^{\mathsf{T}}, \ldots, {}^N\boldsymbol{z}_s^{\mathsf{T}} \right]^{\mathsf{T}}, \tag{3}$$

is a vector of SOP pseudoranges. The estimate $\hat{\boldsymbol{x}}(k+1|k)$ and corresponding prediction error covariance $\mathbf{P}(k+1|k)$ are given by

$$\hat{\boldsymbol{x}}(k+1|k) = \mathbf{F}\hat{\boldsymbol{x}}(k|k) \tag{4}$$

$$\mathbf{P}(k+1|k) = \mathbf{F}\mathbf{P}(k|k)\mathbf{F}^{\mathsf{T}} + \mathbf{Q}, \tag{5}$$

where $\mathbf{F}$ and $\mathbf{Q}$ are the state dynamics matrix and process noise covariance, respectively. Note that since both the vehicles' and SOPs' dynamics are linear, each vehicle may store $\mathbf{F}$ and $\mathbf{Q}$ in memory and compute the time update (4) and (5). Next, the event-based communication strategy and an online test to determine if the packets $\{\boldsymbol{\Lambda}_n\}_{n=1}^N$ should be transmitted are discussed.

C. Event-Based Communication Strategy

This subsection develops an event-based communication strategy, which aims to minimize the transmission rate, while maintaining a desired uncertainty about the vehicle's position. In contrast to all vehicles transmitting $\{\boldsymbol{\Lambda}_n\}_{n=1}^N$ at a fixed rate, which is the rate at which measurements are made; in the event-based strategy, $\{\boldsymbol{\Lambda}_n\}_{n=1}^N$ are only transmitted when a particular event of interest is triggered. In what follows, the event of interest will be defined as the magnitude of any vehicle's position estimation error in any coordinate direction, denoted $|\tilde{x}_{r_n}|$ and $|\tilde{y}_{r_n}|$, violating a specified maximum estimation error $\xi_{\max}$ with probability $1-p$, if transmission of $\{\boldsymbol{\Lambda}_n\}_{n=1}^N$ does not occur. An online test is formulated using the vehicles' position estimation error covariance.

To formulate this test, first consider the normalized estimation error squared (NEES) ϵ_n of the position states for vehicle n, given by

$$\epsilon_n(k) = [\boldsymbol{r}_{r_n}(k) - \hat{\boldsymbol{r}}_{r_n}(k|k)]^{\mathsf{T}}\mathbf{P}_{\boldsymbol{r}_{r_n}}^{-1}(k|k)[\boldsymbol{r}_{r_n}(k) - \hat{\boldsymbol{r}}_{r_n}(k|k)], \tag{6}$$

where $\mathbf{P}_{\boldsymbol{r}_{r_n}}(k|k)$ is the position estimation error covariance for vehicle n. Time dependency will be dropped in the sequel to simplify the notation. The covariance matrix $\mathbf{P}_{\boldsymbol{r}_{r_n}}$ has an eigendecomposition given by

$$\mathbf{P}_{\boldsymbol{r}_{r_n}} = \mathbf{U}_n\mathbf{D}\mathbf{U}_n^{\mathsf{T}}, \quad \mathbf{D} = \operatorname{diag}\left[\lambda_{n,1}, \lambda_{n,2}\right], \tag{7}$$

where $\lambda_{n,i}$ is the i^{th} eigenvalue of $\mathbf{P}_{\boldsymbol{r}_{r_n}}$ and $\mathbf{U}_n$ is an orthogonal matrix whose i^{th} column is the i^{th} eigenvector of $\mathbf{P}_{\boldsymbol{r}_{r_n}}$. Substituting (7) into (6) yields

$$\epsilon_n = \boldsymbol{\xi}_n^{\mathsf{T}}\mathbf{D}^{-1}\boldsymbol{\xi}_n, \tag{8}$$

$$\boldsymbol{\xi}_n \triangleq \mathbf{U}^{\mathsf{T}}(\boldsymbol{r}_{r_n} - \hat{\boldsymbol{r}}_{r_n}). \tag{9}$$

The vector $\boldsymbol{\xi}_n = [\xi_{n,1}, \xi_{n,2}]^{\mathsf{T}}$ is the estimation error $\tilde{\boldsymbol{r}}_{r_n}$ expressed in frame $\{G\}$, rotated by the orthogonal (rotation) matrix $\mathbf{U}^{\mathsf{T}}$ into a coordinate frame $\{F\}$, whose axes coincide with the principal axes of an ellipse. This ellipse is known as the probability concentration ellipse $\mathcal{C}$, which represents the probability p of the error $\boldsymbol{\xi}_n$ lying on or within this ellipse, where

$$p = \Pr\left(\epsilon_n \leq \eta_n\right). \tag{10}$$

Given p and the distribution of ϵ_n, the value η_n can be determined [20]. Therefore, it suffices to check if the largest radii of this ellipse is greater than the specified $\xi_{\max}$.

The principal axes of the confidence ellipse $\mathcal{C}$ are found by expanding (8) and substituting ϵ_n into $\epsilon_n \leq \eta_n$ from (10), which gives

$$\frac{\xi_{n,1}^2}{\eta_n\lambda_{n,1}} + \frac{\xi_{n,2}^2}{\eta_n\lambda_{n,2}} \leq 1, \tag{11}$$

which is the equation of an ellipse with radii $\sqrt{\eta_n\lambda_{n,i}}$, for $i = 1, 2$. These relationships are illustrated in Fig. 2.

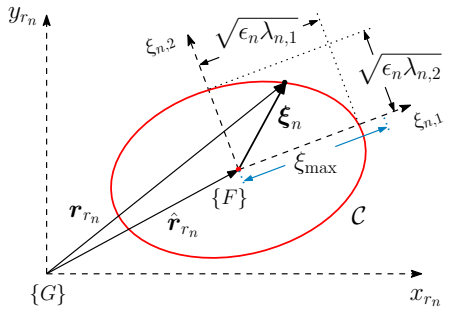

Fig. 2. Probability concentration ellipse $\mathcal{C}$ with origin $\hat{\boldsymbol{r}}_{r_n}$ and radii $\sqrt{\epsilon_n\lambda_{n,i}}$, $i = 1, 2$.

The online test may now be expressed as checking if

$$\sqrt{\eta_n\lambda_{\max}[\mathbf{P}_{\boldsymbol{r}_{r_n}}]} \leq \xi_{\max}, \tag{12}$$

where $\lambda_{\max}[\mathbf{X}]$ denotes the maximum eigenvalue of $\mathbf{X}$. Noting that $\lambda_{\max}[\mathbf{P}_{\boldsymbol{r}_{r_n}}] = \|\mathbf{P}_{\boldsymbol{r}_{r_n}}\|_2$ for covariance matrices and by solving (12) in terms of the specified constraint yields

$$\|\mathbf{P}_{\boldsymbol{r}_{r_n}}\|_2 \leq \frac{\xi_{\max}^2}{\eta_n}. \tag{13}$$

To use test (13) to determine if the specified constraint $\xi_{\max}$ will be violated with probability $1-p$ if the transmission of $\boldsymbol{\Lambda}_n$ does not take place, each vehicle first computes their prediction error covariance, which is given by

$$\mathbf{P}_{\boldsymbol{r}_n}(k+1|k) = \mathbf{F}_{r_n}\mathbf{P}_{r_n}(k|k)\mathbf{F}_{r_n}^{\mathsf{T}} + \mathbf{Q}_{r_n}. \tag{14}$$

The block $\mathbf{P}_{\boldsymbol{r}_{r_n}}$ of (14) is then checked to satisfy (13), i.e.,

$$\|\mathbf{P}_{\boldsymbol{r}_{r_n}}(k+1|k)\|_2 \leq \frac{\xi_{\max}^2}{\eta_n}, \quad n = 1, \ldots, N. \tag{15}$$

If this test fails for any vehicle, the vehicle whose test fails requests all vehicles to transmit their $\boldsymbol{\Lambda}_n$. Subsequently, each vehicle performs an EKF measurement update using its own pseudorange measurements and the communicated packets from other vehicles. If the test does not fail, the measurements are discarded and the measurement update step is skipped. An

event-trigger threshold on the EKF-produced 2σ error standard deviations of the vehicles' position states, over which the transmission of $\{\mathbf{\Lambda}_n\}_{n=1}^N$ is requested, can be found by taking the square root of (15), which yields

$$2\sigma \leq 2\frac{\xi_{\max}}{\sqrt{\eta_n}}. \tag{16}$$

D. EKF Measurement Update

This subsection outlines the EKF measurement update for fusing SOP pseudoranges and packets received from all vehicles, for both fixed-rate and event-based strategies. Upon receiving the packets $\{\mathbf{\Lambda}_n\}_{n=1}^N$, each vehicle assembles the measurement set (3) and uses its locally-generated state prediction (4) to compute the measurement prediction $\hat{\boldsymbol{z}}(k+1|k) \triangleq \mathbb{E}[\boldsymbol{z}(k+1)|\boldsymbol{Z}^k]$. Then, each vehicle computes the estimation correction and corresponding correction error covariance, which are the same for the fixed-rate and event-based strategies when an event triggers the transmission of $\{\mathbf{\Lambda}_n\}_{n=1}^N$, which are given by

$$\begin{aligned}\hat{\boldsymbol{x}}(k+1|k+1) &= \hat{\boldsymbol{x}}(k+1|k)+\mathbf{K}(k+1)[\boldsymbol{z}(k+1) - \hat{\boldsymbol{z}}(k+1|k)]\\ \mathbf{P}(k+1|k+1) &= \mathbf{P}(k+1|k) - \mathbf{K}(k+1)\mathbf{H}(k+1)\mathbf{P}(k+1|k),\end{aligned}$$

$$\begin{aligned}\mathbf{K}(k+1) &\triangleq \mathbf{P}(k+1|k)\mathbf{H}^{\mathsf{T}}(k+1)\mathbf{S}^{-1}(k+1)\\ \mathbf{S}(k+1) &\triangleq \mathbf{H}(k+1)\mathbf{P}(k+1|k)\mathbf{H}^{\mathsf{T}}(k+1) + \mathbf{R},\end{aligned}$$

where $\mathbf{H}$ is the measurement Jacobian evaluated at the state prediction $\hat{\boldsymbol{x}}(k+1|k)$, and $\mathbf{R}$ is the measurement noise covariance of (3). In the event-based strategy, if an event is not triggered, none of the vehicles perform an EKF measurement update and instead continue performing time updates to produce $\hat{\boldsymbol{x}}(k+L|k)$ and $\mathbf{P}(k+L|k)$, where $L = 2, 3, \ldots$.

IV. Simulation Results

This subsection presents simulation results demonstrating the event-based communication strategy and compares its resulting estimation performance and communication rate with a fixed-rate communication strategy. To this end, an environment consisting of $N = 4$ vehicle-mounted receivers and $M = 6$ SOP transmitters was simulated. The vehicles' positions were set to evolve according to a constant turn rate model [16], with

$$\mathbf{F}_{\mathrm{pv}_n} \equiv \begin{bmatrix} 1 & 0 & \frac{\mathtt{s}(\omega T)}{\omega} & -\frac{1-\mathtt{c}(\omega T)}{\omega} \\ 0 & 1 & \frac{1-\mathtt{c}(\omega T)}{\omega} & \frac{\mathtt{s}(\omega T)}{\omega} \\ 0 & 0 & \mathtt{c}(\omega T) & -\mathtt{s}(\omega T) \\ 0 & 0 & \mathtt{s}(\omega T) & \mathtt{c}(\omega T) \end{bmatrix},$$

$$\mathbf{Q}_{\mathrm{pv}_n} \equiv$$

$$S_w \begin{bmatrix} 2\frac{\omega T-\mathtt{s}(\omega T)}{\omega^3} & 0 & \frac{1-\mathtt{c}(\omega T)}{\omega^2} & \frac{\omega T-\mathtt{s}(\omega T)}{\omega^2} \\ 0 & 2\frac{\omega T-\mathtt{s}(\omega T)}{\omega^3} & -\frac{\omega T-\mathtt{s}(\omega T)}{\omega^2} & \frac{1-\mathtt{c}(\omega T)}{\omega^2} \\ \frac{1-\mathtt{c}(\omega T)}{\omega^2} & -\frac{\omega T-\mathtt{s}(\omega T)}{\omega^2} & T & 0 \\ \frac{\omega T-\mathtt{s}(\omega T)}{\omega^2} & \frac{1-\mathtt{c}(\omega T)}{\omega^2} & 0 & T \end{bmatrix},$$

where $\mathtt{s}(\cdot)$ and $\mathtt{c}(\cdot)$ denote $\sin(\cdot)$ and $\cos(\cdot)$, respectively, ω is a known constant turn rate, S_w is the process noise power spectral density, and $n = 1, \ldots, 6$. The coordinates of the SOP transmitters' positions $\{\boldsymbol{r}_{s_m}\}_{m=1}^6$ and the trajectories that the vehicles traversed are illustrated in Fig. 3. The simulation settings are tabulated in Table I.

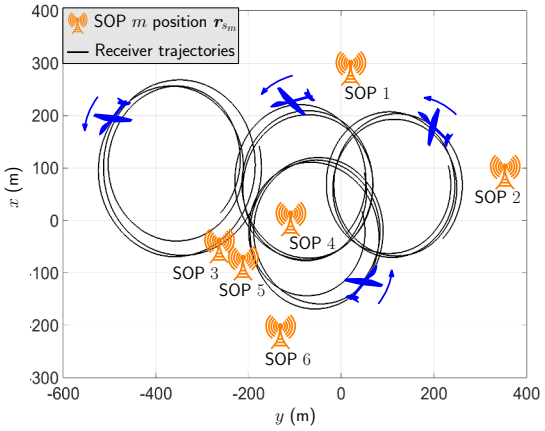

Fig. 3. True trajectories the vehicles traversed (black) and SOP transmitters' positions (orange).

TABLE I
Simulation Settings

Parameter	Value
$\boldsymbol{r}_{r_1}(0)$	$[-220,\ -34]^{\mathsf{T}}$
$\boldsymbol{r}_{r_2}(0)$	$[41,\ -120]^{\mathsf{T}}$
$\boldsymbol{r}_{r_3}(0)$	$[-260,\ 14]^{\mathsf{T}}$
$\boldsymbol{r}_{r_4}(0)$	$[10,\ -25]^{\mathsf{T}}$
$\{\boldsymbol{x}_{\mathrm{clk},r_n}(0)\}_{n=1}^4$	$[10,\ 1]^{\mathsf{T}}$
$\{\boldsymbol{x}_{\mathrm{clk},s_m}(0)\}_{m=1}^6$	$[10,\ 1]^{\mathsf{T}}$
$\mathbf{P}_{\mathrm{clk},s_m}(0\|0)$	$(10^2)\cdot\mathrm{diag}\,[30, 3]$
$\mathbf{P}_{\mathrm{clk},s}(0\|0)$	$\mathrm{diag}\,[\mathbf{P}_{\mathrm{clk},s_1},\ldots\mathbf{P}_{\mathrm{clk},s_6}]$
$\mathbf{P}(0\|0)$	$\mathrm{diag}\,[\mathbf{0}_{24\times 24}, \mathbf{P}_{\mathrm{clk},s}]$
$\hat{\boldsymbol{x}}(0\|0)$	$\sim\mathcal{N}[\boldsymbol{x}(0), \mathbf{P}(0\|0)]$
$\{h_{0,r_n}, h_{-2,r_n}\}_{n=1}^4$	$\{9.4\times10^{-20},\ 0\}$
$\{h_{0,s_m},\ h_{-2,s_m}\}_{m=1}^6$	$\{8.0\times10^{-20},\ 0\}$
ω	0.1 rad/s
T	0.1 s
S_w	$0.01\ \mathrm{m}^2.\mathrm{rad}^2/\mathrm{s}^3$
$\{{}^n\sigma_{s_m}^2\}_{m=1}^5, n = 1,\ldots,4$	$2\ \mathrm{m}^2$

The thresholds specified on the vehicles' position estimates were set to be $\xi_{\max} \equiv 10$ m with a confidence probability $p \equiv 0.999$. The probability density function (pdf) of ϵ_n was found by running 5000 Monte Carlo runs using the environment illustrated in Fig. 3, with random process noise, measurement noise, and initial estimates. The value of η_n in (10) was found using the inverse cumulative distribution function (cdf) of ϵ_n and $p = 0.999$, which evaluated to be $\eta_n \approx 13.8$. Fig. 4 illustrates the Monte Carlo runs histogram of ϵ_n for vehicle 1, from which it was deduced that the pdf follows a gamma distribution with shape and scale parameters $s_1 = 3/2$ and $\theta_1 = 2$, respectively. Plugging η_n and $\xi_{\max}$ into (15) yields $\|\mathbf{P}_{\boldsymbol{r}_{r_1}}(k+1|k)\|_2 \leq 1.81$. The pdf of ϵ_n and

corresponding shape and scale parameters were noted to be the same for the other vehicles.

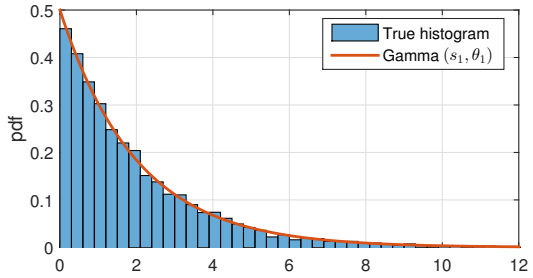

Fig. 4. Histogram of ϵ_1 and gamma distribution with parameters $s_1 = 3/2$ and $\theta_1 = 2$.

The cumulative transmitted data was recorded for each strategy by summing the number of transmitted bits each time a packet transmission occurred. The size of the packet in bits was found by summing the number of values in (2) and setting each value to be a 32-bit float data type, as described in [19]. Fig. 5 shows the resulting estimation errors and corresponding $\pm 2\sigma$ bounds of vehicle 1 along with the $\pm 2\sigma$ bound event-trigger thresholds (16). The resulting cumulative transmitted data for each strategy is illustrated in Fig. 6. Similar plots were noted for the other three vehicles.

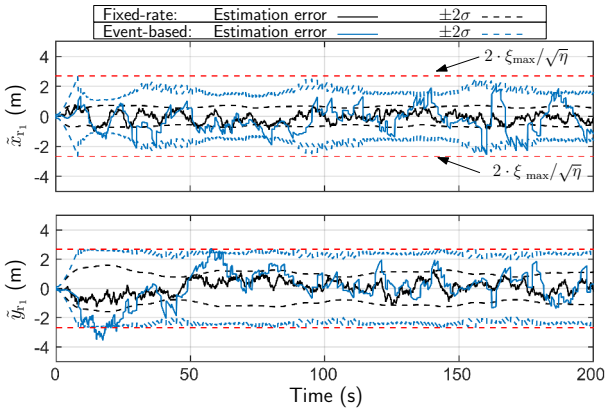

Fig. 5. Resulting estimation errors and corresponding $\pm 2\sigma$ bounds for vehicle 1 for the event-based and fixed-rate communication strategies.

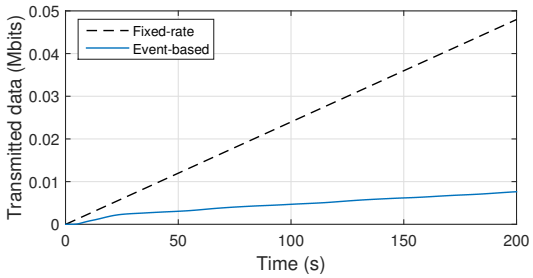

Fig. 6. Cumulative transmitted data for transmitting the packet $\mathbf{\Lambda}_1$ at a fixed-rate and using the event-based communication strategy.

The following may be concluded from these plots. First, note from Fig. 5 that the estimation uncertainties associated with the event-based communication strategy are consistently larger than the ones produced by the fixed-rate strategy. This is due to skipped measurement updates when the test (15) is satisfied. The degradation in estimation performance by skipping these measurements is captured by the distance between the corresponding $\pm 2\sigma$ bounds. Second, as desired, the estimation uncertainties in Fig. 5 in the event-based strategy were below the event-trigger threshold specified in (16). Third, from Fig. 6, the event-based transmission strategy was found to reduce the required total transmitted bits by 86.2% compared to a fixed-rate strategy.

V. Experimental Results

A field experiment was conducted using two UAVs equipped with consumer-grade inertial measurement units (IMUs) and software-defined radios (SDRs) to demonstrate the event-based communication strategy discussed in Section III. To this end, two antennas were mounted on each UAV to acquire and track GPS signals and multiple cellular transmitters, whose signals were modulated through code division multiple access (CDMA). The GPS signals were coupled with the IMU data to produce a navigation solution that served as the ground truth. The cellular signals were downmixed and sampled via Ettus® E312 universal software radio peripherals (USRPs). These front-ends fed their data to the Multichannel Adaptive TRansceiver Information eXtractor (MATRIX) SDR, which produced pseudorange measurements to three cellular transmitters [21]. Fig. 7 depicts the hardware and software setup and Fig. 8 illustrates the experimental environment.

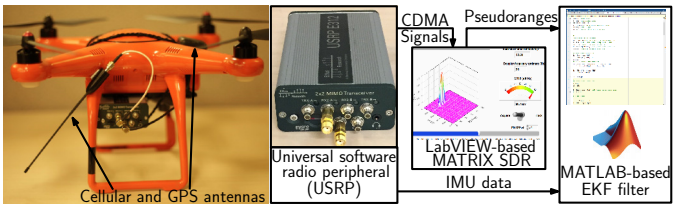

Fig. 7. Experimental hardware setup.

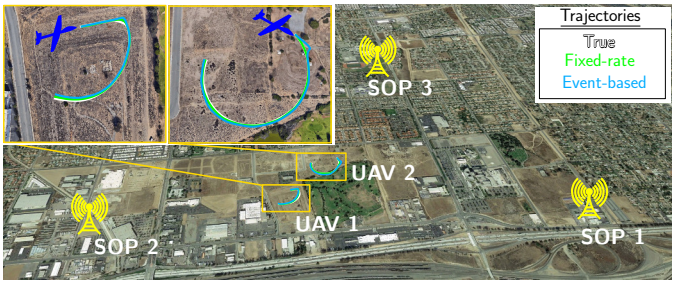

Fig. 8. Experimental environment and navigation results with three cellular SOP transmitters and two UAVs for fixed-rate and event-based transmission strategies.

Two transmission strategies were studied: (i) fixed-rate at $T = 0.1$ and (ii) event-based with $\xi_{\max} \equiv 20$ m and $p \equiv 0.95$, as described in Section III. The UAVs traversed the white trajectories plotted in Fig. 8. To estimate these trajectories, only the cellular SOP pseudoranges were used. The initial state

estimates of the UAVs $\{\hat{\boldsymbol{x}}_r(0|0)\}_{n=1}^2$ were set to the solutions provided by the UAVs' onboard GPS-INS at the beginning of their trajectories, and were assumed to be perfectly known, i.e., $\{\mathbf{P}_{r_n}(0|0)\}_{n=1}^2 \equiv \mathbf{0}_{6\times 6}$. The SOPs' initial clock biases and drifts

$$\boldsymbol{x}_{\text{clk},s_m}(0) = c\left[\delta t_{s_m}(0),\, \dot{\delta} t_{s_m}(0)\right]^{\mathsf{T}} \quad m = 1, \ldots, 3,$$

were solved for by using the initial set of cellular transmitter pseudoranges (1) and the known UAVs' states. The position and velocity states of the UAVs were assumed to evolve according to velocity random walk dynamics with

$$\mathbf{F}_{\text{pv}_n} \equiv \begin{bmatrix} \mathbf{I}_{2\times 2} & T\mathbf{I}_{2\times 2} \\ \mathbf{0}_{2\times 2} & \mathbf{I}_{2\times 2} \end{bmatrix},$$

$$\mathbf{Q}_{\text{pv}_n} \equiv \begin{bmatrix} \frac{T^3}{3}\mathbf{S}_{\text{pv}} & \frac{T^2}{2}\mathbf{S}_{\text{pv}} \\ \frac{T^2}{2}\mathbf{S}_{\text{pv}} & T\mathbf{S}_{\text{pv}} \end{bmatrix}, \quad n = 1, 2,$$

where $\mathbf{S}_{\text{pv}_n} = \text{diag}\,[0.1, 0.1]$ is the process noise power spectral density matrix, whose value was found empirically. The pseudorange measurement noise was assumed to be independent and identically-distributed with covariance $\mathbf{R} = 10 \cdot \mathbf{I}_{6\times 6}$, whose value was found empirically.

The north-east root mean squared error (RMSE) for the fixed-rate transmission strategy for UAV 1 and UAV 2 was 6.0 and 5.2, respectively, and transmitted 7.8 Mbits of data. The north-east root mean squared error (RMSE) for the event-based transmission strategy for UAV 1 and UAV 2 was 10.8 and 6.4, respectively, and transmitted 7.0 Mbits of data. It was noted that that the event-based transmission strategy reduced the transmitted data by 10.3% compared to the the fixed-rate strategy, while maintaining the specified $\xi_{\max}$ and p. Note that in this experiment only three cellular SOPs were exploited to estimate the trajectories of the UAV's. A more significant reduction percentage of transmitted data is expected had (1) additional SOPs been included and (2) the IMU was used in the EKF time update step instead of the simple dynamics model assumed for the UAVs, which inevitably suffers from mismatch with the UAV's true dynamics model.

VI. Conclusion

This paper presented an event-based transmission strategy to share and fuse SOP pseudorange measurements when a specified maximum error in any coordinate direction would be violated with a specified probability. An online event test was developed using each vehicles' position estimation error covariance and was shown in simulation to reduce the transmitted data by 86.2% compared to a fixed-rate strategy. Moreover, experimental results demonstrated two UAVs navigating with the event-based transmission strategy, which reduced the transmitted data by 10.3% compared to a fixed-rate strategy, while maintaining the specified maximum error and probability.

References

[1] C. Yang, T. Nguyen, and E. Blasch, "Mobile positioning via fusion of mixed signals of opportunity," *IEEE Aerospace and Electronic Systems Magazine*, vol. 29, no. 4, pp. 34–46, April 2014.

[2] Z. Kassas, J. Morales, K. Shamaei, and J. Khalife, "LTE steers UAV," *GPS World Magazine*, vol. 28, no. 4, pp. 18–25, April 2017.

[3] S. Fang, J. Chen, H. Huang, and T. Lin, "Is FM a RF-based positioning solution in a metropolitan-scale environment? A probabilistic approach with radio measurements analysis," *IEEE Transactions on Broadcasting*, vol. 55, no. 3, pp. 577–588, September 2009.

[4] Z. Kassas, J. Khalife, K. Shamaei, and J. Morales, "I hear, therefore I know where I am: Compensating for GNSS limitations with cellular signals," *IEEE Signal Processing Magazine*, pp. 111–124, September 2017.

[5] P. Thevenon, S. Damien, O. Julien, C. Macabiau, M. Bousquet, L. Ries, and S. Corazza, "Positioning using mobile TV based on the DVB-SH standard," *NAVIGATION, Journal of the Institute of Navigation*, vol. 58, no. 2, pp. 71–90, 2011.

[6] J. Morales, J. Khalife, A. Abdallah, C. Ardito, and Z. Kassas, "Inertial navigation system aiding with Orbcomm LEO satellite Doppler measurements," in *Proceedings of ION GNSS Conference*, September 2018, accepted.

[7] C. Yang and A. Soloviev, "Covariance analysis of spatial and temporal effects of collaborative navigation," *NAVIGATION, Journal of the Institute of Navigation*, vol. 61, no. 3, pp. 213–225, 2014.

[8] J. Morales, J. Khalife, and Z. Kassas, "Collaborative autonomous vehicles with signals of opportunity aided inertial navigation systems," in *Proceedings of ION International Technical Meeting Conference*, January 2017, 805–818.

[9] Z. Kassas, "Analysis and synthesis of collaborative opportunistic navigation systems," Ph.D. dissertation, The University of Texas at Austin, USA, 2014.

[10] J. Morales and Z. Kassas, "Distributed signals of opportunity aided inertial navigation with intermittent communication," in *Proceedings of ION GNSS Conference*, September 2017, pp. 2519–2530.

[11] Y. Yilmax, G. Moustakides, and X. Wang, "Spectrum sensing via event-triggered sampling," in *Proceedings of Asilomar Conference on Signals, Systems and Computers*, 2011, pp. 1420–1424.

[12] C. Yang, L. Shi, and W. Ma, "A study of estimation and communication tradeoff using an event-based approach," in *Proceedings of Asilomar Conference on Signals, Systems and Computers*, 2013, pp. 32–36.

[13] D. Shi, T. Chen, and L. Shi, "Event-triggered maximum likelihood state estimation," *Automatica*, vol. 50, no. 1, pp. 247–254, 2014.

[14] S. Trimpe and R. D'Andrea, "Event-based state estimation with variance-based triggering," *IEEE Transactions on Automatic Control*, vol. 59, no. 12, pp. 3266–3281, December 2014.

[15] A. Thompson, J. Moran, and G. Swenson, *Interferometry and Synthesis in Radio Astronomy*, 2nd ed. John Wiley & Sons, 2001.

[16] X. Li and V. Jilkov, "Survey of maneuvering target tracking. Part I: Dynamic models," *IEEE Transactions on Aerospace and Electronic Systems*, vol. 39, no. 4, pp. 1333–1364, 2003.

[17] Z. Kassas and T. Humphreys, "Observability analysis of collaborative opportunistic navigation with pseudorange measurements," *IEEE Transactions on Intelligent Transportation Systems*, vol. 15, no. 1, pp. 260–273, February 2014.

[18] J. Morales and Z. Kassas, "Optimal collaborative mapping of terrestrial transmitters: receiver placement and performance characterization," *IEEE Transactions on Aerospace and Electronic Systems*, vol. 54, no. 2, pp. 992–1007, April 2018.

[19] J. Morales and Z. Kassas, "A low communication rate distributed inertial navigation architecture with cellular signal aiding," in *Proceedings of IEEE Vehicular Technology Conference*, 2018, pp. 1–6.

[20] D. Torrieri, "Statistical theory of passive location systems," *IEEE Transactions on Aerospace and Electronic Systems*, vol. 20, no. 2, pp. 183–198, March 1983.

[21] J. Khalife, K. Shamaei, and Z. Kassas, "Navigation with cellular CDMA signals – part I: Signal modeling and software-defined receiver design," *IEEE Transactions on Signal Processing*, vol. 66, no. 8, pp. 2191–2203, April 2018.